

Efficient computational models for shallow water flows over multilayer erodible beds

Thomas Rowan*, Mohammed Seaid†

Abstract

Numerical modeling of shallow water flows over heterogeneous sedimentary layers is presented. The governing equations consist of the well-established shallow water equations for the flow, a transport equation for the suspended sediments, an Exner-type equation for the bed load and a set of empirical equations for erosion and deposition terms. Multi-layered beds formed with different erodible soils are considered in this study. It is already several years since the single-layered models have used to model shallow water flows over erodible beds. Although such models present a real opportunity for shallow water flows over movable beds but this work is the first to propose a multi-layered solver for this class of flow problems. For the numerical solution of the coupled system we consider a non-homogeneous Riemann solver equipped with interface-tracking tools to resolve discontinuous soil properties in the multi-layered bed. The solver consists of a predictor stage for the discretization of gradient terms and a corrector stage for the treatment of source terms. Numerical results are presented for several test examples of shallow water flows over sedimentary layers. The obtained results demonstrate that the proposed method preserves the conservation property and it provides accurate results avoiding numerical oscillations and numerical dissipation in the approximated solutions.

Keywords. Shallow water flows; Sedimentary layers; Suspended sediment; Finite volume method; Riemann solver

1 Introduction

The primary intent of sediment transport (or morphodynamics) is to determine the evolution of bed levels for hydrodynamic systems such as rivers, estuaries, bays and other near-shore regions where water flows interact with the bed geometry. Examples of applications include: beach profile changes due to severe wave actions, seabed response to dredging procedures or imposed structures and harbor siltation Zhang et al. (2017); Abderrezzak et al. (2013); Cao and Pender (2004); Li and Duffy (2011). In general, suspended sediments and bed-load transport in shallow water flows are determined by the characteristics of the hydraulic flow and the properties of the suspended sediments. Thus, dynamics of the water and dynamics of the sediments must be studied using a mathematical model formed of three different but dependent model variables: (i) a set of hydraulic variables defining the dynamics of the water flow, (ii) a sediment variable defining the transport and dispersion of the sediments and (iii) a topography variable defining the dynamics of the bed-load. Most existing models for this class of problems consider either the three-dimensional Navier-Stokes equations or a depth-averaged system widely known by shallow water equations for the hydrodynamics coupled to a class of Exner-type equations for the sediment load, compare Capart and Young (1998); Abbott (1979); Terzaghi et al. (1996); Liu and A. (2017) and further references

*School of Engineering, University of Durham, South Road, Durham DH1 3LE, UK (thomas.rowan@durham.ac.uk)

†School of Engineering, University of Durham, South Road, Durham DH1 3LE, UK (m.seaid@durham.ac.uk)

are therein. The difficulties in the first approach are seen by the re-meshing required to deal with moving boundaries for free-surface and bottom topography due to the hydrostatic pressure and erosion/deposition forces. Because of its high computational cost, this approach is rarely used in practical applications. The drawback in the second approach lies in the failure of the coupled shallow water system and the Exner equations to capture vertical effects in a soil-superposed packed bed.

The understanding of morphological evolution due to shallow water flows is crucial to the development of river defenses and flood control Kondolf et al. (2014); Vercruysse et al. (2017). The ability to accurately simulate a range of situations, from near steady-state bed degradation to dam-break conditions is very important to the design and maintenance of flood defenses and hydro-infrastructures Abderrezzak et al. (2013). Many scientific efforts have been made to develop good understanding of the interaction between water flows and movable beds by accurately modelling entrainment and deposition rates. A set of formula for entrainment was first proposed in Shields (1936). Although many good categorizations have been introduced in the literature, a unified theory has yet to be found, see for example Brownlie (1981); Paphitis (2001). For modelling morphodynamics in shallow water flows, the three most popular models are the Grass model Grass (1981), the Meyer-Peter & Muller model Meyer-Peter and Müller (1948) and the Van-Rijn model Van Rijn (1984). In this paper we shall use the erosion and deposition formula proposed in Cao and Pender (2004); Van Rijn (1984) as they are best suited to the problems considered. One of the most complicated aspects of simulating sediment transport is the correct modeling of the bed due to the number of assumptions required such as the levels of armoring, vegetation, composition and compaction. This often leads to a large disconnect between laboratory experiments and simulations when compared to real-world measurements. Recently corrections have been investigated in Chen et al. (2017); Mohtar et al. (2016); Sanford (2008) to improve these assumptions. However, homogeneous assumption on the erodible beds is one of the severe limitation in these models as there is no situation (outside the laboratory) where the bed is truly homogeneous. Developing models for multiple sediments has been also discussed in Rowan and Seaid (2016) but the research field remains underdeveloped. In the current study we present a new coupled model for hydraulics over multi-layered erodible beds. The bed is assumed to be heterogeneous and formed with multiple layers of different soil properties. The structure of soil-superposed packed beds and the total number of layers to be considered in the analysis are fixed a priori.

In the current study, the governing equations consist of a coupled system of shallow water equations for the hydraulics, a transport equation for suspended sediments, an Exner-type equation for the bed load, and a series of exchange terms for the mass transfer between the bed layers due to erosion and/or deposition effects. These equations form a nonlinear hyperbolic system of balance laws with source terms to be solved for the time interval, the horizontal space coordinate, and the vertical bed depth. Such practical coupled hydrodynamical and morphodynamical problems are not trivial to simulate since the soil can be heterogeneous and the topography irregular. It should be pointed out that other mathematical models for sediment transport have also been studied in Liang et al. (2003); Kozyrakis (2016) among others. In these systems, the shallow water equations have been coupled to an Exner-type equation for the bed-load which do not account for suspended sediments as shown in the current study. In this paper we present a fully coupled model for shallow water flows over multi-layered and mixed sediment erodible beds. In the present work, the Exner equation for the bed is modified to allow for inter-cellular flux in the vertical discretization of the bed depth. The bed layers can be assumed to be heterogeneous and composed of multiple layers of different sediment mixtures. The structure of the soil-superposed packed beds is assumed to be initially known along with the number of layers in the model. Combined with the sediment handling tools and a two-dimensional discretized bed, multiple sediments can be eroded, deposited or remain stationary within the same cell depending on the properties of sediments under study. The novelty of the present work lies on the introduction of a flux function for the bed in the vertical

direction to allow for multiple sediments and on the development of a consistent model similar to the Saint-Venant-Hirano model Siviglia et al. (2017) to handle multilayers in discretized beds. Crucially the approach is designed to impact the complexity of the model as little as possible and therein the computational expense.

Development and design numerical methods that are able to predict the hydraulics over multi-layered erodible beds has clear mathematical and engineering relevances. Nowadays, much effort has been devoted to implement numerical schemes for sediment transport models capable of resolving all hydrodynamics and morphodynamics scales. Here, a class of Riemann solvers is proposed for the numerical simulation of transient flows involving erosion and deposition of sediments in the multi-layered beds. The proposed method also satisfies the C-property by well-balancing the discretization of flux gradients and source terms in the system. Using a similar approach as in Rowan and Seaid (2016) we developed interface tracking tools to account for initially mixed sediments. This allows for the comparison of initial sediment assumptions as shown in this paper. A second-order accuracy is achieved in the proposed solver using flux limiters in the same manner as described in Benkhaldoun et al. (2012). To analyze the effectiveness of the proposed techniques, we first compare our computational results to experimental data for the test example of a dam-break flow over erodible bed reported in Capart and Young (1998), and for the problem of the degradation of a Dyke studied in Guan et al. (2015). Next we simulate similar flow problems over erodible multi-layered beds and examine the performance of the proposed techniques using different numbers of layers in the sedimentary topography. These examples also highlighted the interchangeability of sediment erosion and deposition equations. Results presented in this paper demonstrate high resolution of the proposed method and confirm its capability to provide accurate and efficient simulations for sediment transport by water flows including erosion and deposition effects in heterogeneous beds.

This paper is organized as follows: In Section 2 we briefly present the governing equations for shallow water flows over sedimentary topography. Modeling exchange terms between multi-layered beds is discussed in Section 3. In Section 4 we formulate the Riemann solver for both the discretization of gradient fluxes and the treatment of source terms. Numerical results and examples are presented in Section 5. Finally, Section 6 contains some concluding remarks.

2 Shallow water flows over sedimentary topography

The conventional governing equations of sediment transport in shallow water flows are obtained by balancing the net inflow of mass, momentum, and species through boundaries of a control volume. This is achieved during an infinitesimal time interval while accounting for the accumulation of mass, resultant forces and species within the control volume Abbott (1979); Cao and Carling (2002). These equations can be formulated in a conservative form as

$$\begin{aligned}
\frac{\partial h}{\partial t} + \frac{\partial(hu)}{\partial x} &= \frac{E - D}{1 - p}, \\
\frac{\partial(hu)}{\partial t} + \frac{\partial}{\partial x} \left(hu^2 + \frac{1}{2}gh^2 \right) &= -gh \frac{\partial B}{\partial x} - \frac{(\rho_s - \rho_w)}{2\rho} gh^2 \frac{\partial c}{\partial x} - \frac{(\rho_0 - \rho)(E - D)u}{\rho(1 - p)} - ghS_f, \\
\frac{\partial(hc)}{\partial t} + \frac{\partial(huc)}{\partial x} &= E - D, \\
\frac{\partial B}{\partial t} &= -\frac{E - D}{1 - p},
\end{aligned} \tag{1}$$

where $u(t, x)$ is the depth-averaged water velocity, $h(t, x)$ the water depth, $B(t, x)$ the bottom topography, g the gravitational acceleration, p the porosity, ρ_w the water density, ρ_s the sediment density, c the depth-averaged concentration of the suspended sediment, E and D represent the

total entrainment and deposition terms in upward and downward directions, respectively. Here, S_f is the friction slope defined as

$$S_f = \frac{m_n^2 u |u|}{h^{4/3}}, \quad (2)$$

where m_n is the Manning roughness coefficient. In (1), ρ and ρ_0 are respectively, the density of the water-sediment mixture and the density of the saturated bed defined by

$$\rho = \rho_w(1 - c) + \rho_s c, \quad \rho_0 = \rho_w p + \rho_s(1 - p). \quad (3)$$

Notice that equations (1) have been widely used in the literature to model sediment transport, see for instance Abbott (1979); Cao et al. (2004); Hu and Cao (2009); Benkhaldoun et al. (2012) and further references are therein. These equations can be rewritten in a canonical vector form as

$$\frac{\partial \mathbf{U}}{\partial t} + \frac{\partial \mathbf{F}(\mathbf{U})}{\partial x} = \mathcal{S}(\mathbf{U}) + \mathcal{Q}(\mathbf{U}), \quad (4)$$

where

$$\mathbf{U} = \begin{pmatrix} h \\ hu \\ hc \\ B \end{pmatrix}, \quad \mathbf{F}(\mathbf{U}) = \begin{pmatrix} hu \\ hu^2 + \frac{1}{2}gh^2 \\ huc \\ 0 \end{pmatrix},$$

$$\mathcal{S}(\mathbf{U}) = \begin{pmatrix} 0 \\ -gh \frac{\partial B}{\partial x} - \frac{(\rho_s - \rho_w)}{2\rho} gh^2 \frac{\partial c}{\partial x} \\ 0 \\ 0 \end{pmatrix}, \quad \mathcal{Q}(\mathbf{U}) = \begin{pmatrix} \frac{E - D}{1 - p} \\ -\frac{(\rho_0 - \rho)(E - D)u}{\rho(1 - p)} - ghS_f \\ E - D \\ -\frac{E - D}{1 - p} \end{pmatrix}.$$

The system (4) can also be rearranged in a non-conservative form as

$$\frac{\partial \mathbf{U}}{\partial t} + \mathcal{A}(\mathbf{U}) \frac{\partial \mathbf{U}}{\partial x} = \mathcal{S}(\mathbf{U}) + \mathcal{Q}(\mathbf{U}), \quad (5)$$

where

$$\mathcal{A}(\mathbf{U}) = \begin{pmatrix} 0 & 1 & 0 & 0 \\ gh - u^2 - \frac{(\rho_s - \rho_w)}{2\rho} ghc & 2u & \frac{(\rho_s - \rho_w)}{2\rho} gh & gh \\ -uc & c & u & 0 \\ 0 & 0 & 0 & 0 \end{pmatrix}.$$

It is easy to verify that the system (4) is hyperbolic in nature with four real and distinct eigenvalues of the matrix \mathcal{A} given by

$$\lambda_1 = 0, \quad \lambda_2 = u, \quad \lambda_3 = u - \sqrt{gh}, \quad \lambda_4 = u + \sqrt{gh}, \quad (6)$$

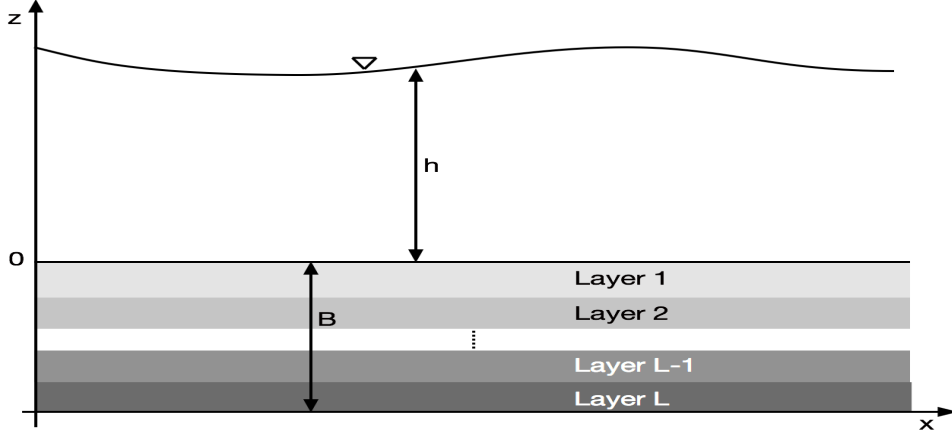


Figure 1: Sketch of a system of shallow-water flow over a multi-layered bed.

and their corresponding eigenvectors are

$$e_1 = \begin{pmatrix} -gh \\ 0 \\ -ghc \\ gh - u^2 \end{pmatrix}, \quad e_2 = \begin{pmatrix} \frac{\rho_s - \rho_w}{2\rho} \\ \frac{\rho_s - \rho_w}{2\rho} u \\ \frac{\rho_s - \rho_w}{2\rho} c - 1 \\ 0 \end{pmatrix}, \quad e_3 = \begin{pmatrix} 1 \\ u - \sqrt{gh} \\ c \\ 0 \end{pmatrix}, \quad e_4 = \begin{pmatrix} 1 \\ u + \sqrt{gh} \\ c \\ 0 \end{pmatrix}.$$

Note that in all the studies cited above, the sediment transport system (4) is solved for homogeneous beds formed of a single type of soil. However, for many realistic applications in sediment transport by shallow water flows the topography is constituted of multiple soils and in many cases superposed in layers. Therefore, we are interested in situations of shallow water flows over multi-layered beds as shown in Figure 1. Thus, the bottom topography depends also on the vertical direction z *i.e.*, $B = B(t, x, z)$. We consider a system where multiple species of sediments ($k = 1, 2, \dots, N$) exist in a number of layers ($l = 1, 2, \dots, L$) with N and L refer to the total number of sediment species and the total number of layers in the bed, respectively. Note that two layers may contain the same sediment species or a layer may contain multiple sediment species. For simplicity, we use the cumulative sediment concentration

$$\bar{c} = \sum_{k=1}^N c_k.$$

Subsequently, we also introduce the averaged variables

$$\bar{\rho}_s = \sum_{k=1}^N \frac{c_k}{\bar{c}} \rho_{s,k}, \quad \bar{\rho} = \rho_w(1 - \bar{c}) + \sum_{k=1}^N \frac{c_k}{\bar{c}} \rho_{s,k}, \quad \bar{D} = \sum_{k=1}^N \frac{c_k}{\bar{c}} D_k. \quad (7)$$

For the remaining variables $\bar{\rho}_0$, \bar{E} and \bar{p} we use the equivalent averaging with respect to sediments in the bed associated with the active cell. To ascertain the composition of the bed we discretize the vertical direction into a set of control volumes $[z_{j-1/2}, z_{j+1/2}]$ ($j = 1, 2, \dots, J$) with uniform size Δz for simplicity only, see Figure 2 for an illustration. Each control volume may contain different sediment species which need to be organized in a rigorous manner to be compatible with the governing equations. Here, the active top cell has a height B_j formed of three sediments. For

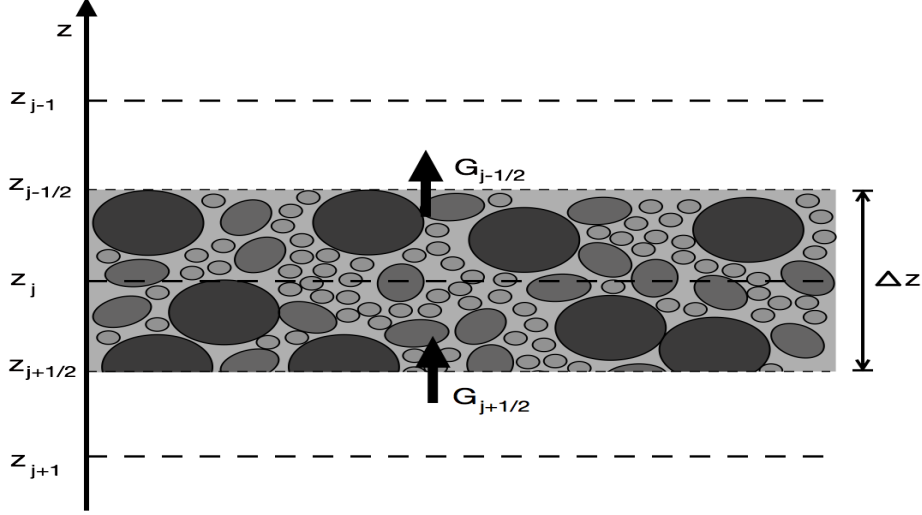


Figure 2: Vertical discretization of the bed into control volumes $[z_{j+1/2}, z_{j-1/2}]$.

example, in three-layered bed, the equivalent height of each of the three sediments is $b_{j,1}$, $b_{j,2}$ and $b_{j,3}$. Thus, the proportion of each sediment type in the bed γ_1 may be represented as

$$B_j = b_{j,1} + b_{j,2} + b_{j,3}, \quad b_{j,1} = B_j \gamma_1.$$

Hence, the bed-dependent variables are calculated using the weighted averaging procedure Terzaghi et al. (1996) as

$$\bar{p}_j = \sum_{k=1}^N \frac{b_{j,k}}{B_j} p_k, \quad \bar{\rho}_{0,j} = \rho_w (1 - \bar{p}) + \sum_{k=1}^N \frac{b_{j,k}}{B_j} \rho_k, \quad \bar{E} = \sum_{k=1}^N \frac{b_{j,k}}{B_j} E_k. \quad (8)$$

Balancing the exchange forces in each control volume shown in Figure 2 we obtain the bed-load equation

$$\frac{\partial B}{\partial t} + \frac{\partial G(B)}{\partial z} = - \frac{\bar{E} - \bar{D}}{1 - \bar{p}}, \quad (9)$$

where $G(B)$ is a flux function which depends on the exchange terms between the bed cells and it is discussed below in Section 3. Note that each cell interacts only with its two neighboring cells whereas, erosion and deposition only occur in the active top cell. Thus, the equations we consider in the present study for modeling shallow water flows over multi-layered beds read

$$\begin{aligned} \frac{\partial h}{\partial t} + \frac{\partial (hu)}{\partial x} &= \frac{\bar{E} - \bar{D}}{1 - \bar{p}}, \\ \frac{\partial (hu)}{\partial t} + \frac{\partial}{\partial x} \left(hu^2 + \frac{1}{2} gh^2 \right) &= -gh \frac{\partial B}{\partial x} - \frac{(\bar{\rho}_s - \bar{\rho}_w)}{2\bar{\rho}} gh^2 \frac{\partial c}{\partial x} - \frac{(\bar{\rho}_0 - \bar{\rho})(\bar{E} - \bar{D})u}{\bar{\rho}(1 - \bar{p})} - ghS_f, \\ \frac{\partial (h\bar{c})}{\partial t} + \frac{\partial hu\bar{c}}{\partial x} &= \bar{E} - \bar{D}, \\ \frac{\partial B}{\partial t} + \frac{\partial G(B)}{\partial z} &= - \frac{\bar{E} - \bar{D}}{1 - \bar{p}}. \end{aligned} \quad (10)$$

In what follows we describe the equations used to model the erosion terms E and the deposition terms D . Most formula for models of suspended sediments, obtained from experiments and

measured data, are empirical to differing extents. For detailed discussions on the mathematical and physical aspects of the considered sediment formula, we refer to Cao and Pender (2004); Cao et al. (2006); Simpson and S. (2006) among others. In addition, to determine the entrainment and deposition terms in the above equations we assume non-cohesive sediments and we use empirical relations reported in Li and Duffy (2011); Cao and Carling (2002). Thus, for a given sediment k

$$D_k = \omega_{s,k} \alpha_{c,k} c_k, \quad (11)$$

where α_c is a coefficient larger than unity to ensure that the near-bed concentration does not exceed the value of $(1 - p)$. Here the coefficient α_c is computed as in Cao et al. (2004) by the relation

$$\alpha_{c,k} = \min \left(2, \frac{1 - p_k}{c_k} \right).$$

In (11), ω_s is the settling velocity of a single particle in tranquil water defined as

$$\omega_{s,k} = \frac{\sqrt{(36\nu_k/d_k)^2 + 7.5\rho_s g d - 36\nu/d}}{2.8}, \quad (12)$$

with ν_k is the kinematic viscosity of the water, d_k the average diameter of the sediment particles. For the erosion term E_k we also employed the equations suggested in Cao and Pender (2004)

$$E_k = \begin{cases} \varphi_k \frac{\theta_k - \theta_{c,k}}{h} u d_k^{-0.2}, & \text{if } \theta_k \geq \theta_{c,k}, \\ 0, & \text{otherwise,} \end{cases} \quad (13)$$

where φ is a coefficient to control the erosion forces, θ_c is a critical value of Shields parameter for the initiation of sediment motion and θ is the Shields coefficient defined by

$$\theta = \frac{u_*^2}{s_k g d_k}, \quad (14)$$

with $s = \rho_{s,k}/\rho_w - 1$ is the submerged specific gravity of sediment and $u_{*,k}$ is the friction velocity defined using the Darcy-Weisbach friction factor f_k as

$$u_{*,k}^2 = \sqrt{\frac{f_k}{8}} |u|.$$

It should be stressed that the erosion terms (13) are not suitable for problems with low shear sediment transport. In this case, the system can be assumed at equilibrium and the following erosion terms suggested in Van Rijn (1984) are considered

$$E_k = \begin{cases} 0.0033 \rho_s \sqrt{\Delta g d_k} d_*^{0.3} \tau^{1.5}, & \text{if } u_* > u_{*,cr}, \\ 0, & \text{otherwise,} \end{cases} \quad (15)$$

where d_* is the dimensionless diameter of the particle and τ is a transport-stage parameter defined as

$$d_* = d_{50} \left(\frac{\Delta g}{\nu^2} \right)^{1/3}, \quad \tau = \frac{(u_*^2) - (u_{*,cr}^2)}{(u_{*,cr}^2)}.$$

Note that the equations (10) can also be rearranged in the compact vector form (5). Note that other empirical formula for the erosion and deposition terms can also be used in our Riemann solver without major conceptual modifications. It should also be stressed that since the flux function added in the bed-load is only differentiated with respect to z , the hyperbolic parts in the system (10) are not changed from those appearing in its conventional counterpart (1). Therefore, the eigenvalues and eigenvectors associated with the system (10) are also given by the expressions (6).

3 Modeling the exchange terms for multi-layered beds

Let us discretize the bottom topography into control volumes $[z_{j+1/2}, z_{j-1/2}]$ with same length Δz as shown in Figure 2. We also divide the time interval into subintervals $[t_n, t_{n+1}]$ with uniform size Δt . Here, $t_n = n\Delta t$, $z_{j+1/2} = j\Delta z$ and $z_j = (j - 1/2)\Delta z$ is the center of the control volume. Following the standard finite volume formulation, we integrate the bed-load equation (9) with respect to time and space over the domain $[t_n, t_{n+1}] \times [z_{j+1/2}, z_{j-1/2}]$ to obtain the following discrete equation

$$B_j^{n+1} = B_j^n + \frac{\Delta t}{\Delta z} \left(G_{j+1/2}^n - G_{j-1/2}^n \right) + \Delta t S_j^n, \quad (16)$$

where B_j^n is the space depth-averaged bed B given in equation (1) and evaluated in the control volume $[z_{j+1/2}, z_{j-1/2}]$ at time t_n *i.e.*,

$$B_j^n(x) = \frac{1}{\Delta z} \int_{z_{j+1/2}}^{z_{j-1/2}} B(t_n, x, z) dz,$$

and $G_{j\mp 1/2}^n = G(B_{j\mp 1/2}^n)$ are the numerical fluxes at $z = z_{j\mp 1/2}$ and time t_n . Since the erosion and deposition takes place only in the top active cell, the source term in (16) is defined as

$$S_j^n = \begin{cases} -\frac{\bar{E}_j^n - \bar{D}_j^n}{1 - \bar{p}_j}, & \text{if } z_{j+1/2} < B_j^n \leq z_{j-1/2}, \\ 0, & \text{elsewhere.} \end{cases} \quad (17)$$

It should be noted that as $0 \leq B_j^n \leq \Delta z$ only four possible cases illustrated in Figure 3 may occur for erodible beds. These cases are:

- 1) Cell growth. Erosion and deposition rates in the cell do not exceed the cell bounds.
- 2) Cell depletion. The cell is entirely eroded and the cell below becomes active.
- 3) Cell overfill. The cell is overfilled and the cell above becomes the active cell.
- 4) Cell armoring. The cell holds out against total erosion.

To derive the flux functions $G_{j\mp 1/2}^n$ in (16) we apply boundary conditions for the three first cases of homogeneous sediments and similar process is applied for the heterogeneous sediments, but for the sake of brevity this is omitted here. For example, in the case of cell overfill, $B_j^{n+1} = \Delta z$ and $G_{j+1/2}^n = 0$. Hence,

$$\Delta z = B_j^n + \frac{\Delta t}{\Delta z} \left(-G_{j-1/2}^n \right) + \Delta t S_j^n,$$

which can be rearranged as

$$G_{j-1/2}^n = \frac{\Delta z}{\Delta t} \left(B_j^n - \Delta z - \Delta t \frac{\bar{E}_j^n - \bar{D}_j^n}{1 - \bar{p}_j} \right). \quad (18)$$

For the case of cell depletion, $B_j^{n+1} = 0$ and $G_{j-1/2}^n = 0$. Hence,

$$0 = B_j^n + \frac{\Delta t}{\Delta z} \left(G_{j+1/2}^n \right) + \Delta t S_j^n,$$

which can be rearranged as

$$G_{j-1/2}^n = \frac{\Delta z}{\Delta t} \left(-B_{j-1}^n + \Delta t \frac{\bar{E}_{j-1}^n - \bar{D}_{j-1}^n}{1 - \bar{p}_{j-1}} \right). \quad (19)$$

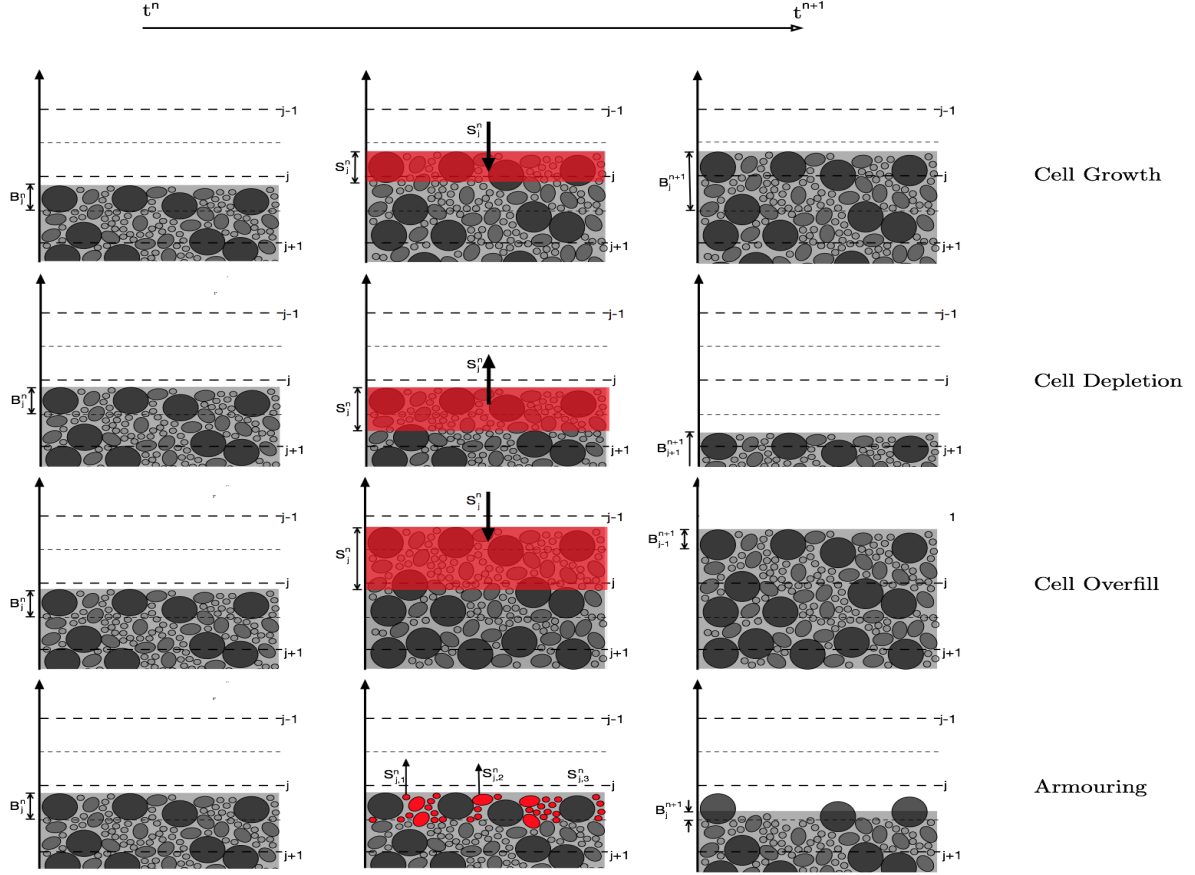


Figure 3: Illustration of different cell alterations for shallow water flows over erodible beds. Red color is used to highlight entrained or deposited sediments. For the top three options it is assumed that all sediment is entrained together and for last option, armoring or hiding occurs as only the finer sediments are eroded.

For the case of cell growth, both upper and lower fluxes vanish and

$$G_{j-1/2}^n = \begin{cases} \frac{\Delta z}{\Delta t} \left(B_j^n - \Delta z - \Delta t \frac{\bar{E}_j^n - \bar{D}_j^n}{1 - \bar{p}_j} \right), & \text{if } B_j^n - \Delta t \frac{\bar{E}_j^n - \bar{D}_j^n}{1 - \bar{p}_j} > \Delta z, \\ \frac{\Delta z}{\Delta t} \left(-B_{j-1}^n + \Delta t \frac{\bar{E}_{j-1}^n - \bar{D}_{j-1}^n}{1 - \bar{p}_{j-1}} \right), & \text{if } B_j^n - \Delta t \frac{\bar{E}_{j-1}^n - \bar{D}_{j-1}^n}{1 - \bar{p}_{j-1}} < 0, \\ 0, & \text{otherwise.} \end{cases} \quad (20)$$

Note that this approach requires only the evaluation of bed height in the three neighboring cells and it can be implemented for homogeneous beds using the test bed height

$$B_{*,j}^{n+1} = B_j^n - \Delta t \frac{\bar{E}_j^n - \bar{D}_j^n}{1 - \bar{p}_j}.$$

Given the bed B_j^n at time t_n , the bed B_j^{n+1} at time t_{n+1} is updated using Algorithm 1.

For the cell armoring, the sediment mixes between the bed and the flow, and to handle this we assume that the cell height can be expressed as the sum of the heights of the sediments inside it as

Algorithm 1: Procedure to update the bed in the homogeneous multi-layered situation

```

if  $B_{*,j}^{n+1} > \Delta z$  then
  |  $B_j^{n+1} = \Delta z$ 
  |  $B_{j-1}^{n+1} = B_j^n - \Delta z - \Delta t \frac{E_j^n - D_j^n}{1 - p_j}$ 
else if  $B_{*,j}^{n+1} \leq 0$  then
  |  $B_j^{n+1} = 0$ 
  |  $B_{j+1}^{n+1} = B_j^n + \Delta z - \Delta t \frac{E_j^n - D_j^n}{1 - p_j}$ 
else
  |  $B_j^{n+1} = B_{*,j}^{n+1}$ 
end

```

shown in Figure 3. For this case, we calculate the bed height $b_{*,j,k}$ at each time step as

$$b_{*,j,k}^{n+1} = b_{j,k}^n + \Delta b_{j,k}^n = b_{j,k}^n + \Delta t \left(\frac{E_{j,k}^n - D_{j,k}^n}{1 - p_{j,k}} \right),$$

where $b_{j,k}$ ($k = 1, 2, \dots, N$) are the corresponding heights of sediment contained within the cell. We also define $\Delta b_{*,j}^-$ and $\Delta b_{*,j}^+$ as the sum of all the negative and all positive $\Delta b_{j,k}$ sediment height changes in the cell, respectively. Hence, the procedure to update and all $b_{j,k}$ ($k = 1, 2, \dots, N$) the bed b_j^{n+1} for this case is described in Algorithm 2.

There are four possible cases considered in Algorithm 2 and realized by considering four possible outcomes:

- 1) **Cell overflow:** where the cell is overfilled and the cell above becomes the active cell. The deposition of sediment plus the initial quantity of sediment is so great that the cell is no longer in direct contact with the water but the cell above it is now partially filled and consequently becomes the active cell. This is achieved by checking the proposed new total bed height $B_{*,j}^{n+1} \geq \Delta z$, if not the next condition is checked.
- 2) **Cell armouring:** where the cell holds out against total erosion. One or more sediment types have been totally eroded from the cell, but one or more other sediment types remain in the cell protecting the cell beneath from contact with the water. This condition is evaluated by checking if any sediment still remains in the cell $b_{*,j,k}^{n+1} \geq 0$ and if the cell would be completely eroded $\sum_{k=1}^N b_{*,j,k}^{n+1} \leq 0$ then the height changes are re-calculated based on the cell beneath not being touched.
- 3) **Cell depletion:** where the cell is entirely eroded and the cell below becomes active. All sediment within the cell is removed so that the sediment in the cell below is now in contact with the water. If neither of the above two conditions is met then we check that all of $b_{*,j,k}^{n+1} \geq 0$, this activates the cell depletion algorithm, where sediment in the cell below is then eroded in this time step.
- 4) **Cell growth:** where erosion and deposition rates in the cell do not exceed the cell bounds. The net movement of sediment together with the original amount of sediment remains within the bounds of the cell. Finally if none of the other options have been activated then $b_{j,k}^{n+1} = b_{*,j,k}^{n+1}$, as this is the only other option available.

Algorithm 2: Procedure to update the bed in the non-homogeneous multi-layered situation

```

if  $\sum_{k=1}^N b_{*,j,k}^{n+1} \geq \Delta z$  then
  for  $k = 1 : N$  do
    if  $b_{*,j,k}^{n+1} \geq 0$  then
      
$$b_{j,k}^{n+1} = b_{j,k}^n + (\Delta z - B_j^n - \Delta b_{*,j}^-) \frac{\Delta b_{*,j,k}^n}{\Delta b_{*,j}^+ - \Delta b_{*,j}^-}$$

      
$$b_{j-1,k}^{n+1} = \Delta b_{*,j,k}^{n+1} - (\Delta z - B_j^n - \Delta b_{*,j}^-) \frac{\Delta b_{*,j,k}^n}{\Delta b_{*,j}^+ - \Delta b_{*,j}^-}$$

    else
       $b_{j,k}^{n+1} = b_{*,j,k}^{n+1}$ 
    end
  end
end

else if any  $k \in \{1, \dots, N\}$   $b_{*,j,k}^{n+1} \geq 0$  and  $\sum_{k=1}^N b_{*,j,k}^{n+1} \leq 0$  then
  for  $k = 1 : N$  do
    if  $b_{*,j,k}^{n+1} > 0$  then
       $b_{j,k}^{n+1} = b_{*,j,k}^{n+1}$ 
    else
       $b_{j,k}^{n+1} = 0$ 
       $\Delta b_{*,j,k}^n = -b_{j,k}^n$ 
    end
  end
end

else if all  $b_{*,j,k}^{n+1} \leq 0$  then
  for  $k = 1 : N$  do
    if  $b_{*,j+1,k}^n > 0$  then
       $b_{j+1,k}^{n+1} = b_{j,k}^n + b_{j+1,k}^n - \Delta b_{*,j,k}^n$ 
    else
       $\Delta b_{*,j,k}^n = -b_{j,k}^n$ 
    end
     $b_{j,k}^{n+1} = 0$ 
  end
end

else
  for  $k = 1 : N$  do
     $b_{j,k}^{n+1} = b_{*,j,k}^{n+1}$ 
  end
end

```

It is worth mentioning that for the case of cell armoring, inappropriate discretization of the bed may have a direct effect on the morphodynamics. For a well graded soil it is possible to set a lower limit on the vertical discretization using the largest particle size d . For other types of soils, it is suggested to account for the d_{99} fraction which is usually considered an order of magnitude greater than d_{50} . Therefore for the multi-layered discretization, where armoring is possible, the following constraint is recommended

$$\Delta z \geq 10d_{50}. \quad (21)$$

Note that composition of the layered beds should be known in advance but the number of discretized layers in the algorithm can be set by the user and two or more discretized layers may be formed with the same soil.

4 Riemann solver for the multi-layered beds

For the finite volume discretization of the system (4) we discretize the spatial domain into control volumes $[x_{i-1/2}, x_{i+1/2}]$ with uniform size Δx for sake of simplicity. Here, $x_{i-1/2} = i\Delta x$ and $x_i = (i + 1/2)\Delta x$ is the center of the control volume. Integrating the equation (4) with respect to time-space over the domain $[t_n, t_{n+1}] \times [x_{i-1/2}, x_{i+1/2}]$ we obtain the following discrete system

$$\mathbf{U}_i^{n+1} = \mathbf{U}_i^n - \frac{\Delta t}{\Delta x} \left(\mathbf{F}(\mathbf{U}_{i+1/2}^n) - \mathbf{F}(\mathbf{U}_{i-1/2}^n) \right) + \Delta t \mathcal{S}(\mathbf{U}_i^n) + \Delta t \mathcal{Q}(\mathbf{U}_i^n), \quad (22)$$

where \mathbf{U}_i^n is the space average of the solution \mathbf{U} in the control volume $[x_{i-1/2}, x_{i+1/2}]$ at time t_n defined as

$$\mathbf{U}_i^n = \frac{1}{\Delta x} \int_{x_{i-1/2}}^{x_{i+1/2}} \mathbf{U}(t_n, x) dx,$$

and $\mathbf{F}(\mathbf{U}_{i\pm 1/2}^n)$ are the numerical fluxes at the interfaces $x = x_{i\pm 1/2}$ and time t_n . The treatment of source terms \mathcal{S} and \mathcal{Q} in (22) is dealt with using the standard splitting procedure Toro (1999)

$$\begin{aligned} \mathbf{U}_i^* &= \mathbf{U}_i^n - \frac{\Delta t}{\Delta x} \left(\mathbf{F}(\mathbf{U}_{i+1/2}^n) - \mathbf{F}(\mathbf{U}_{i-1/2}^n) \right) + \Delta t \mathcal{S}(\mathbf{U}_i^n), \\ \mathbf{U}_i^{n+1} &= \mathbf{U}_i^* + \Delta t \mathcal{Q}(\mathbf{U}_i^*). \end{aligned} \quad (23)$$

To complete the spatial discretization of the equations (23) a reconstruction of the numerical fluxes $\mathbf{F}(\mathbf{U}_{i\pm 1/2}^n)$ and source term $\mathcal{S}(\mathbf{U}_i^n)$ must be selected. In general applications, this reconstruction requires a solution of Riemann problems at the interfaces $x_{i\pm 1/2}$. Here, the self-similar solution to the Riemann problem formed of the equation (4) subject to the initial condition

$$\mathbf{U}(0, x) = \begin{cases} \mathbf{U}_L, & \text{if } x < 0, \\ \mathbf{U}_R, & \text{if } x > 0, \end{cases} \quad (24)$$

is given by

$$\mathbf{U}(t, x) = \mathbf{R}_s \left(\frac{x}{t}, \mathbf{U}_L, \mathbf{U}_R \right),$$

where \mathbf{R}_s is the Riemann solution which can be evaluated analytically for the shallow water equations over fixed beds, see Alcrudo and Benkhaldoun (2001) for the exact expression of \mathbf{R}_s . Thus, the intermediate state $\mathbf{U}_{i+1/2}^n$ in (22) at the cell interface $x_{i+1/2}$ is defined as

$$\mathbf{U}_{i+1/2}^n = \mathbf{R}_s \left(0, \mathbf{U}_i^n, \mathbf{U}_{i+1}^n \right). \quad (25)$$

Note that this procedure is computationally demanding and it may restrict the application of the method for problems which exact Riemann solvers are not available. Furthermore, the discretization

of the source terms in (22) may suffer from singular values raised from the Riemann solver at the interfaces. These difficulties are typical in the numerical solution of shallow water equations over erodible sediment beds and they will be retained for shallow water flows over sedimentary topography. In order to avoid these difficulties and reconstruct an approximation of $\mathbf{U}_{i+1/2}^n$, we adapt a finite volume non-homogeneous Riemann solver proposed in Sahnim et al. (2007) for the numerical solution of shallow water flows over fixed beds. The Riemann solver has also been extended in Benkhaldoun et al. (2012) for solving dam-break problems over erodible beds. In the present work, we examine the performance of the Riemann solver for solving shallow water flows over multi-layered sedimentary beds. Hence, applied to the first step in the splitting (23), the Riemann solver results in a predictor-corrector scheme of the form

$$\begin{aligned}\mathbf{U}_{i+1/2}^n &= \frac{1}{2}(\mathbf{U}_{i+1}^n + \mathbf{U}_i^n) - \frac{1}{2}\text{sgn}\left[\mathcal{A}(\widehat{\mathbf{U}}_{i+1/2}^n)\right](\mathbf{U}_{i+1}^n - \mathbf{U}_i^n), \\ \mathbf{U}_i^* &= \mathbf{U}_i^n - \frac{\Delta t}{\Delta x}\left(\mathbf{F}(\mathbf{U}_{i+1/2}^n) - \mathbf{F}(\mathbf{U}_{i-1/2}^n)\right) + \Delta t\mathcal{S}(\mathbf{U}_i^n),\end{aligned}\tag{26}$$

where the averaged state $\widehat{\mathbf{U}}_{i+1/2}^n$ is calculated as

$$\widehat{\mathbf{U}}_{i+1/2}^n = \begin{pmatrix} \frac{h_i^n + h_{i+1}^n}{2} \\ \frac{\sqrt{h_i^n} u_i^n + \sqrt{h_{i+1}^n} u_{i+1}^n}{\sqrt{h_i^n} + \sqrt{h_{i+1}^n}} \\ \frac{\sqrt{h_i^n} c_i^n + \sqrt{h_{i+1}^n} c_{i+1}^n}{\sqrt{h_i^n} + \sqrt{h_{i+1}^n}} \\ \frac{B_i^n + B_{i+1}^n}{2} \end{pmatrix},\tag{27}$$

and the sign matrix in (26) is given by

$$\text{sgn}\left[\mathcal{A}(\widehat{\mathbf{U}}_{i+1/2}^n)\right] = \mathcal{R}(\widehat{\mathbf{U}}_{i+1/2}^n) \left|\Lambda(\widehat{\mathbf{U}}_{i+1/2}^n)\right|^{-1} \Lambda(\widehat{\mathbf{U}}_{i+1/2}^n) \mathcal{R}^{-1}(\widehat{\mathbf{U}}_{i+1/2}^n).\tag{28}$$

The determination of the sign matrix $\text{sgn}\left[\mathcal{A}(\widehat{\mathbf{U}})\right]$ is carried out using the eigenvalues in (6) as

$$\text{sgn}\left[\mathcal{A}(\widehat{\mathbf{U}})\right] = \mathcal{R}(\widehat{\mathbf{U}}) \text{sgn}\left[\Lambda(\widehat{\mathbf{U}})\right] \mathcal{R}^{-1}(\widehat{\mathbf{U}}),$$

where

$$\text{sgn}\left[\Lambda(\widehat{\mathbf{U}})\right] = \begin{pmatrix} \text{sgn}(\widehat{\lambda}_1) & 0 & 0 & 0 \\ 0 & \text{sgn}(\widehat{\lambda}_2) & 0 & 0 \\ 0 & 0 & \text{sgn}(\widehat{\lambda}_3) & 0 \\ 0 & 0 & 0 & \text{sgn}(\widehat{\lambda}_4) \end{pmatrix},$$

with $\widehat{\lambda}_k$ ($k = 1, 2, 3, 4$) are the eigenvalues in (6) calculated at the averaged state (27). The right and left eigenvector matrices in (28) are defined by

$$\mathcal{R}(\widehat{\mathbf{U}}) = \begin{pmatrix} -\widehat{s}^2 & \widehat{r} & 1 & 1 \\ 0 & \widehat{r}u & \widehat{\lambda}_3 & \widehat{\lambda}_4 \\ -\widehat{s}^2\widehat{c} & \widehat{r}\widehat{c} - 1 & \widehat{c} & \widehat{c} \\ -\widehat{\lambda}_3\widehat{\lambda}_4 & 0 & 0 & 0 \end{pmatrix}, \quad \mathcal{R}^{-1}(\widehat{\mathbf{U}}) = \begin{pmatrix} 0 & 0 & 0 & \frac{-1}{\widehat{\lambda}_3\widehat{\lambda}_4} \\ \widehat{c} & 0 & -1 & 0 \\ \frac{\widehat{\lambda}_4 - \widehat{c}\widehat{r}\widehat{s}}{2\widehat{s}} & \frac{-1}{2\widehat{s}} & \frac{\widehat{r}}{2} & \frac{-\widehat{s}}{2\widehat{\lambda}_3} \\ -\frac{\widehat{\lambda}_3 + \widehat{c}\widehat{r}\widehat{s}}{2\widehat{s}} & \frac{1}{2\widehat{s}} & \frac{\widehat{r}}{2} & \frac{\widehat{s}}{2\widehat{\lambda}_4} \end{pmatrix},$$

where $\widehat{s} = \sqrt{g\widehat{h}}$ is the wave speed and $\widehat{r} = \frac{\rho_s - \rho_w}{2\widehat{\rho}}$ is a density ratio. Using the above matrices, the averaged state $\mathbf{U}_{i+1/2}^n$ can be easily obtained from the predictor stage in (26). Once these states are computed, the solution \mathbf{U}_i^{n+1} is recovered using the corrector stage in (26).

For the the discretization of the source terms \mathcal{S} and \mathcal{Q} in (23) we use the well-balanced method reported in Benkhaldoun et al. (2012). Here the discretization of the source terms is carried out such that the scheme is well balanced with the discretization of the flux gradients using the concept of C-property. Recall that a numerical scheme is said to satisfy the still-water equilibrium (C-property) for the equations (4) if the condition

$$u = 0, \quad B^n = \bar{B}(x), \quad h + B = \text{constant}, \quad (29)$$

holds for stationary flows at rest. Therefore, the treatment of source terms in (26) is reconstructed such that the condition (29) is preserved at the discretized level. Hence, following the same procedure as in Benkhaldoun et al. (2012), the proposed Riemann solver satisfies the C-property if the source terms in the corrector stage of (26) are discretized as

$$\mathcal{S}(\mathbf{U}_i^n) = \begin{pmatrix} 0 \\ -g \frac{h_{i+1/2}^n + h_{i-1/2}^n}{2} \frac{B_{i+1}^n - B_{i-1}^n}{2\Delta x} - \frac{(\bar{\rho}_s - \rho_w)}{2\bar{\rho}_i^n} g \left(\frac{h_{i+1/2}^n + h_{i-1/2}^n}{2} \right)^2 \frac{c_{i+1}^n - c_{i-1}^n}{2\Delta x} \\ 0 \\ 0 \end{pmatrix},$$

$$\mathcal{Q}(\mathbf{U}_i^n) = \begin{pmatrix} \frac{E_i^n - D_i^n}{1 - \bar{p}} \\ -\frac{(\bar{\rho}_0 - \bar{\rho}_i^n)(E_i^n - D_i^n)u_i^n}{\bar{\rho}_i^n(1 - \bar{p})} - g \frac{h_{i+1/2}^n + h_{i-1/2}^n}{2} S_f \\ E_i^n - D_i^n \\ -\frac{E_i^n - D_i^n}{1 - \bar{p}} \end{pmatrix}$$

It should be stressed that the well-balanced discretization is a key for accurate predictions of sediment transport by shallow water flows. In practice, if the C-property is not satisfied by the numerical method then nonphysical oscillations may appear in its numerical solutions. Failure of capturing shocks and presence of instability problems may also occur if the discretization of the

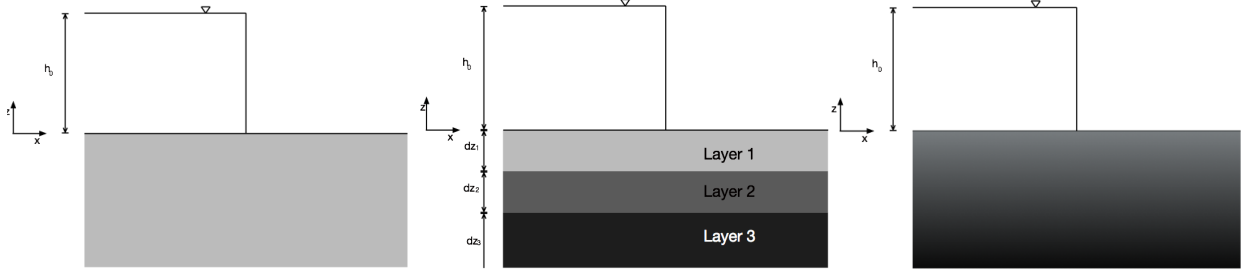


Figure 4: Illustration of a dam-break problem over a single-layered bed (left plot), a three-layered bed (middle plot) and a gradually varying bed (right plot).

flux gradients and the discretization of the source terms are not well balanced. In the current study, we also used flux limiters to achieve a second-order in the finite volume solver. Details on the implementation of these techniques are similar to those discussed in Benkhaldoun et al. (2012) and therefore these details are omitted here. In summary, the solver consists of the following two steps:

Predictor step: In this step intermediate solutions and numerical fluxes are calculated as in (26).

Corrector step: In this step numerical solution is updated using the splitting procedure (23).

Note that the bed height is calculated using equation (16) in the corrector step.

5 Numerical results

We present numerical results for several problems of shallow water flows over multi-layered beds. We consider test examples for both evolving and steady-state flow simulations of homogeneous, non-homogeneous and graded erodible sediment beds using the sediment properties presented in Table 1. These parameters have been used in many sediment transport applications, see for example Van Rijn (2007); Wu and Wang (2006); Rubey (1933). For all results presented in this section $\rho_w = 1000 \text{ kg/m}^3$, $g = 9.81 \text{ m/s}^2$ and $\nu = 1.2 \times 10^{-6} \text{ m}^2/\text{s}$. The main goal of this section is to illustrate the performance of the proposed Riemann solver coupled with the discretized bed in handling these situations. Both simulations are first tested against experimental data for which only homogeneous single-layered beds are solved and then extended to show the effects of varying the bed composition. In all computations, the Courant number $\text{CFL}=0.8$ is used to vary the time step Δt according to the stability condition

$$\Delta t = \text{CFL} \min \left(\frac{\Delta x}{\max_{k=1,2,3,4} (|\lambda_k^n|)} \right),$$

where λ_k ($k = 1, 2, 3, 4$) are the four eigenvalues of the sediment transport system given in (6). Note that the above stability condition takes into account the rate of vertical changes and it ensures that the bed information never jumps more than one vertical cell as long as $\Delta z \leq \Delta x$.

Table 1: Sediment parameters provided in Van Rijn (2007); Wu and Wang (2006); Rubey (1933) for some bed types used in our simulations for the erosion and deposition formula.

Sediment	d [mm]	p	φ	ω_s [m/s]	ρ_s [kg/m ³]	u_{cr} [m/s]	m_n [s/m ^{1/3}]
Sand 1	0.0625	0.5	0.015	0.00014	1650	-	0.012
Sand 2	0.25	0.35	0.015	0.001	1650	-	0.013
Sand 3	0.20	0.4	0.015	0.0015	1600	-	0.013
Sand 4	0.16	0.4	0.075	0.019	2650	0.0145	0.01
Sand 5	0.20	0.4	0.075	0.019	2700	0.0145	0.01
Sand 6	0.25	0.4	0.075	0.020	2800	0.0145	0.01
Pearls	6.1	0.4	0.000015	0.0001	1048	-	0.025

5.1 Results for dam-break problems

We consider dam-break problems over erodible beds formed with homogeneous single-layered sand, heterogeneous three-layered sands, and gradually varying sands as depicted in Figure 4. The selected values for the sediment parameters used for the evaluation of our Riemann solver are given in Table 1. For this evolving flow problem the erosion term is given by the formula (13). Initially, the bottom topography is assumed to be flat (*i.e.* $B(0, x, z) = 0$) and at $t = 0$ the dam breaks and the flow problem yields a shock wave traveling downstream and a rarefaction wave traveling upstream. To validate the numerical results obtained using our Riemann solver to measurements we consider the dam-break experiment detailed in Capart and Young (1998). In this experiment, the channel is 1.2 m long and the bed is assumed to be homogeneously formed by artificial spherical pearls with sediment properties given in Table 1. As initial conditions we set

$$h(0, x) = \begin{cases} 0.1 \text{ m}, & \text{if } x \leq 0, \\ 0.05 \text{ m}, & \text{if } x > 0, \end{cases} \quad u(0, x) = 0 \text{ m/s}, \quad c(0, x) = 0.$$

The spacial domain is discretized into 150 control volumes and results for bed-load and free-surface are presented. In Figure 5 we present a comparison of the computed results and measurements obtained for the bed-load and the water free-surface at time $t = 0.505 \text{ s}$. The agreement between the simulations and measurements is reasonably good. The erosion magnitude and wave-front location are well predicted by our Riemann solver. As expected an hydraulic jump is formed near the initial dam place and propagates upstream along the channel. However, the location of the hydraulic jump is less accurately predicted by the numerical model. This may be attributed to the fact that three-dimensional effects from the experimental set-up have been not accounted for in the numerical problem. Time evolutions of the bed profile and the sediment concentration are presented in Figure 6. As the time evolves, the erosion acts widely on the bed and the eroded material contributes to the sediment concentration. The proposed Riemann solver performs very well for this dam-break problem since it does not diffuse the moving bed and no spurious oscillations have been observed when the water flows over the erodible bed. Furthermore, the obtained results using the proposed Riemann solver compare favorably with those reported in Cao et al. (2004); Simpson and S. (2006) for similar test problem of dam-break flows over erodible beds.

Next, we consider a dam-break problem in a rectangular channel with an heterogeneous bottom

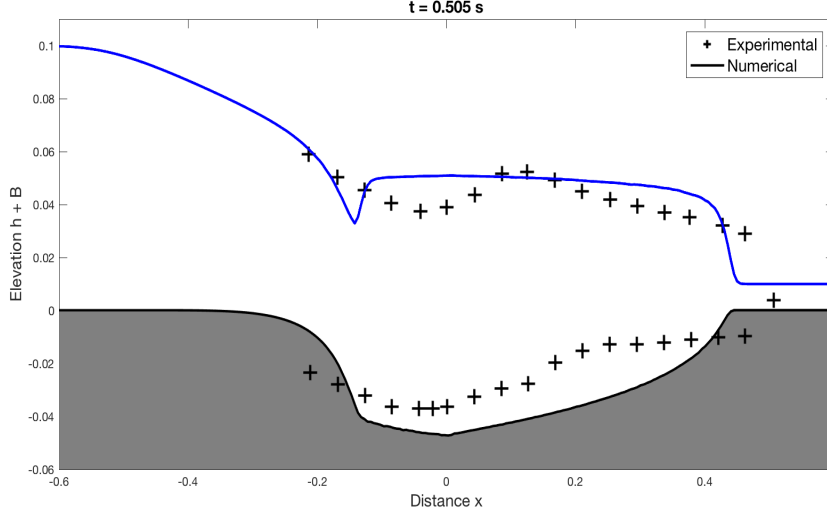


Figure 5: Comparison between numerical results and experimental data for a dam-break problem over single-layered bed at time $t = 0.505 s$.

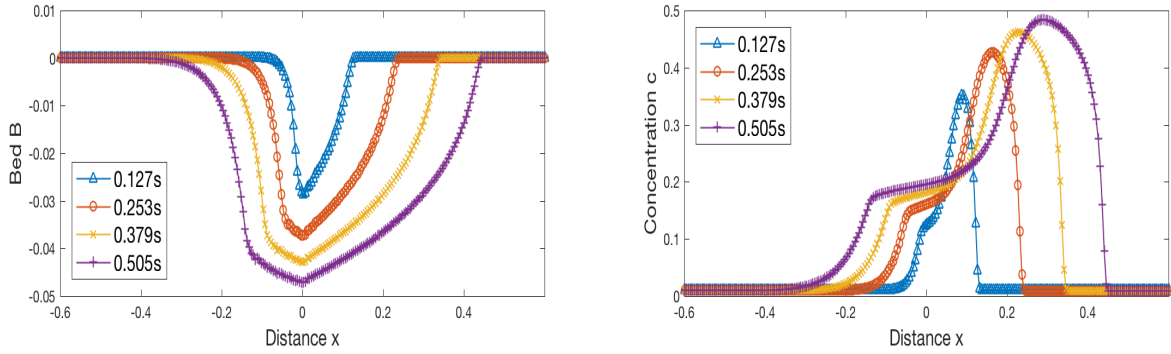


Figure 6: Time evolution of the bed profile (left plot) and the sediment concentration (right plot) for a dam-break problem over the single-layered Taipei experiment bed.

initially assumed to be flat. The channel is of length $1000 m$ and the initial conditions are given by

$$h(0, x) = \begin{cases} 5 m, & \text{if } x \leq 500 m, \\ 0.0001 m, & \text{if } x > 500 m, \end{cases} \quad u(0, x) = 0 m/s, \quad c(0, x) = 0.0001. \quad (30)$$

In order to highlight the effect of making different assumptions on the bed, three situations are simulated namely (i) homogeneous single-layer bed of Sand 2, (ii) heterogeneous three-layered bed of Sand 1, Sand 2 and Sand 3, and (iii) gradually varying bed from Sand 1 to Sand 3. The depth of the bed is $4 m$ and for the three-layered situation it is initially formed by

$$B(0, x, z) = \begin{cases} \text{Sand 1,} & \text{if } -1.25 m \leq z < 0 m, \\ \text{Sand 2,} & \text{if } -2.5 m \leq z < -1.25 m, \\ \text{Sand 3,} & \text{if } -4 m \leq z < -2.5 m. \end{cases}$$

Table 2: CPU times, error in the bed-load, and error in the minimum values of the bed profile using different spatial and bed discretization steps Δx and Δz for the accuracy test problem.

		Horizontal discretization				
		$\Delta x = 3.33 m$	$\Delta x = 2.86 m$	$\Delta x = 2.50 m$	$\Delta x = 2.22 m$	$\Delta x = 2.00 m$
Vertical discretization	$\Delta z = 0.12 m$	203 s	262 s	346 s	438 s	540 s
		8.50 %	5.60 %	2.44 %	1.32 %	0.067 %
		1.62 %	1.10 %	0.74 %	0.34 %	0.01 %
	$\Delta z = 0.060 m$	205 s	261 s	349 s	446 s	553 s
		8.89 %	5.66 %	4.50 %	1.53 %	-0.36 %
		1.57 %	1.11 %	0.64 %	0.35 %	0.01 %
	$\Delta z = 0.030 m$	205 s	268 s	351 s	455 s	567 s
		8.73 %	6.79 %	3.54 %	1.58 %	0.44 %
		1.61 %	1.05 %	0.69 %	0.35 %	0.01 %
	$\Delta z = 0.020 m$	208 s	280 s	363 s	458 s	567 s
		7.96 %	5.75 %	3.46 %	1.13 %	0.08 %
		1.66 %	1.10 %	0.66 %	0.34 %	0.02 %
	$\Delta z = 0.015 m$	208 s	280 s	365 s	461 s	571 s
		7.66 %	5.75 %	3.79 %	1.60 %	—
		1.66 %	1.11 %	0.65 %	0.34 %	—

For the situation of gradually varying bed, the initial bed is formed by a gradual variation from Sand 1 to Sand 3 as

$$B(0, x, z) = \left(\frac{2.5 + z}{2.5} \right) \text{Sand 1} + \left(\frac{z}{-2.5} \right) \text{Sand 3}.$$

We first perform a convergence study for the spatial and bed discretizations to quantify the errors and also to check the effectiveness of the proposed techniques. To this end, we consider the situation of a dam-break problem over homogeneous single-layered bed of Sand 2, which could be interpreted as an average between the two other situations considered in this test example. In order to quantify the errors in this example, a reference solution computed using a fine discretization with $\Delta x = 2 m$ and $\Delta z = 0.015 m$ is used as an exact solution. We compute the solutions at time $t = 20 s$ using different spatial and bed discretizations.

In Table 2 we summarize the errors in the bed-load, the bed profiles and the computational times for each pair of $(\Delta x, \Delta z)$. We use the L^1 -error norm for calculating the errors using the computed reference solution to be as the exact one. The CPU times are included to assess the cost-benefit of mesh refinement in the simulation process. As can be seen from the results presented in this table, increasing the number of control volumes in the horizontal spatial discretization results in an increase in the accuracy and also in the computational cost of the Riemann solver. For the coarse discretization ($\Delta x = 3.33 m, \Delta z = 0.12 m$) the numerical errors are more visible than for the other discretizations. An examination of the obtained results in Table 2 also reveals that, when compared to the horizontal discretization, the vertical discretization has small effects on both the accuracy and the efficiency of the proposed techniques. For example, using $(\Delta x = 2.86 m, \Delta z = 0.12 m)$ the computational time and the error in the suspended load error are respectively 262 s and 1.10 %

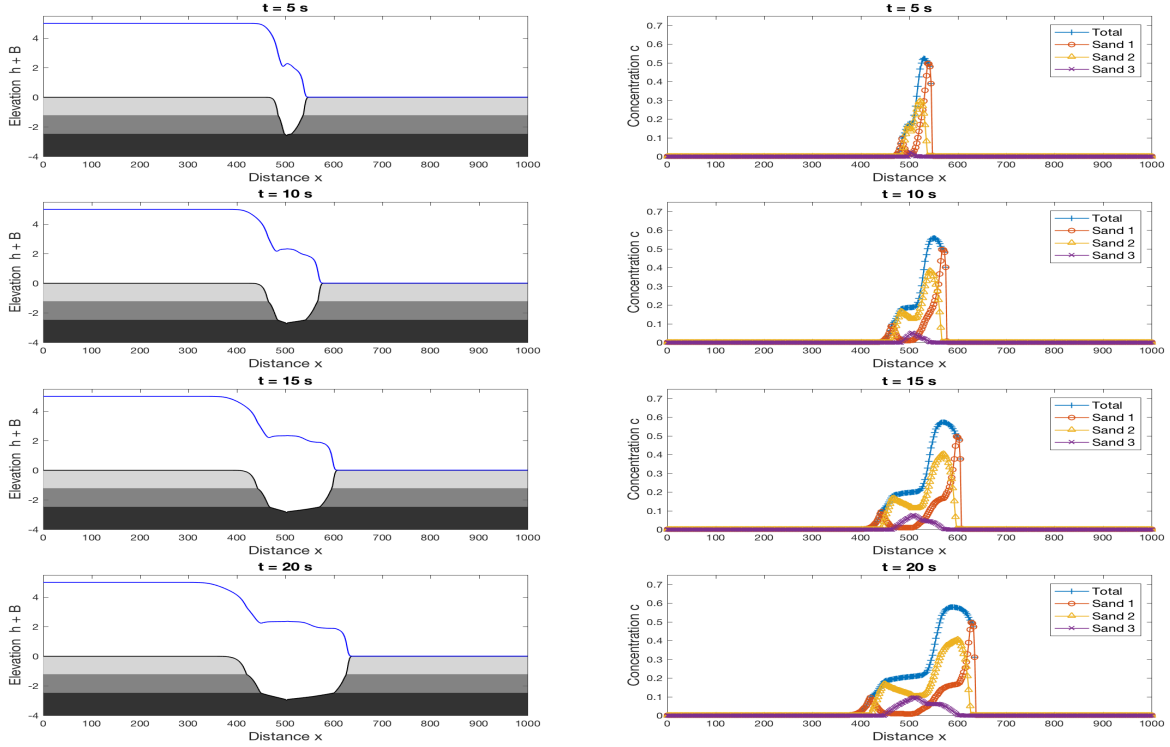


Figure 7: Water heights and bed profiles (left column) and sediment concentrations (right column) for a dam-break problem over a three-layered bed at four different instants.

whereas using ($\Delta x = 2.22 \text{ m}$, $\Delta z = 0.020 \text{ m}$) these results become 458 s and 0.34% . A spatial convergence is clearly achieved in the proposed Riemann solver for both horizontal and vertical discretizations. For the considered flow and sediment conditions, a balance between accuracy and efficiency in our method favored the discretization using ($\Delta x = 2.22 \text{ m}$, $\Delta z = 0.020 \text{ m}$).

Next, we turn our attention to check the performance of our models for dam-break flows over heterogeneous multi-layered beds. To this end, we run the Riemann solver for the three-layered and gradually varying bed using ($\Delta x = 2.22 \text{ m}$, $\Delta z = 0.020 \text{ m}$). Other multi-layered simulations with higher number of layers can also be computed using our model. Figure 7 presents water heights, bed profiles and sediment concentrations for the dam-break problem over a three-layered bed at four different instants $t = 5, 10, 15$ and 20 s . Those results obtained for the dam-break problem over gradually varying bed are presented in Figure 8. Dark and light colors are used in these figures for the bed of Sand 3 and Sand 1, respectively. As can be observed from these results, the dam-break flow over the movable bed can build up a heavily concentrated wave-front which is bounded by the wave forefront and a contact discontinuity of the sediment transport, and it depresses in the long run. The bed mobility can strongly modify the water free-surface profiles and may have considerable implications for flood predictions. As in the previous simulations, an hydraulic jump in the water free-surface is initially formed around the dam site, it depresses progressively as it propagates upstream and eventually disappears. It is evident that the movable bed can be significantly scoured and the dimensions of the scour hole are of similar order of magnitude to those of the water flow itself. Therefore the rate of bed deformation is not negligible compared to that of the flow change, characterizing the need for coupled modeling of the strongly interacting flow-sediment-morphology system, as considered in the present work. From the presented results we can conclude that the proposed Riemann solver performs very well for this dam-break problem since it does not diffuse the moving water fronts and no spurious oscillations have been detected when the dam breaks over the sedimentary bed. Finally, a comparison of the bed profile obtained

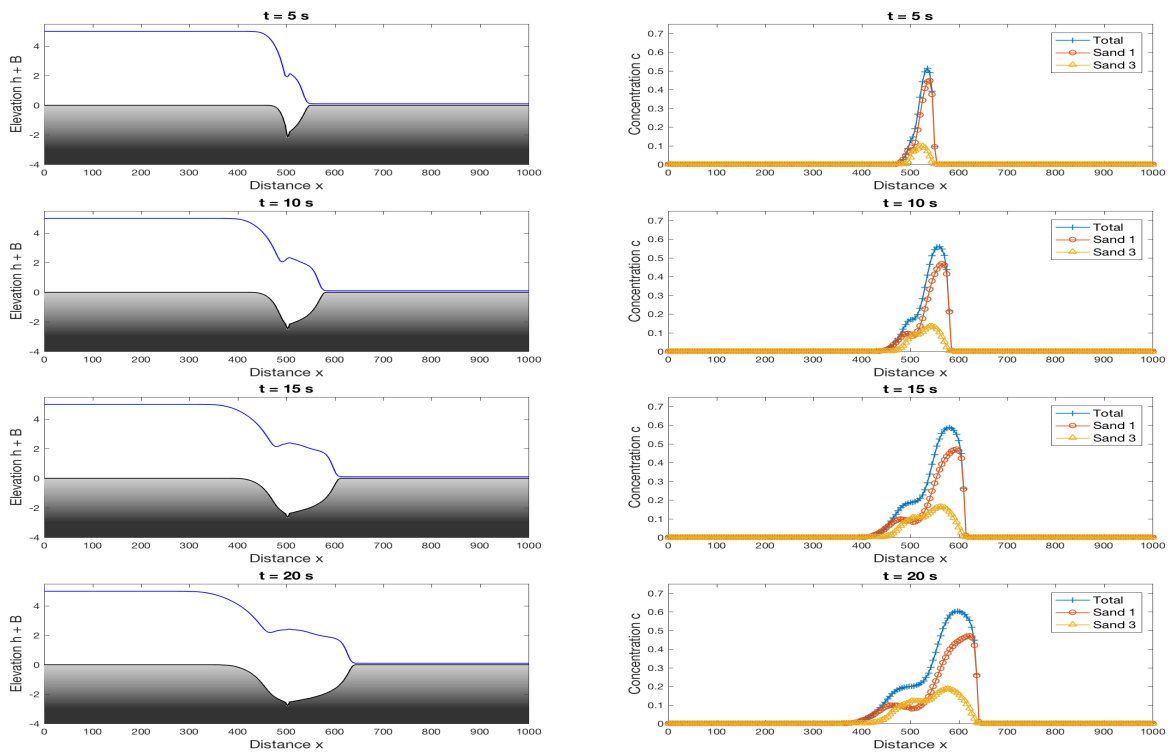


Figure 8: Water heights and bed profiles (left column) and sediment concentrations (right column) for a dam-break problem over a gradually varying bed at four different instants.

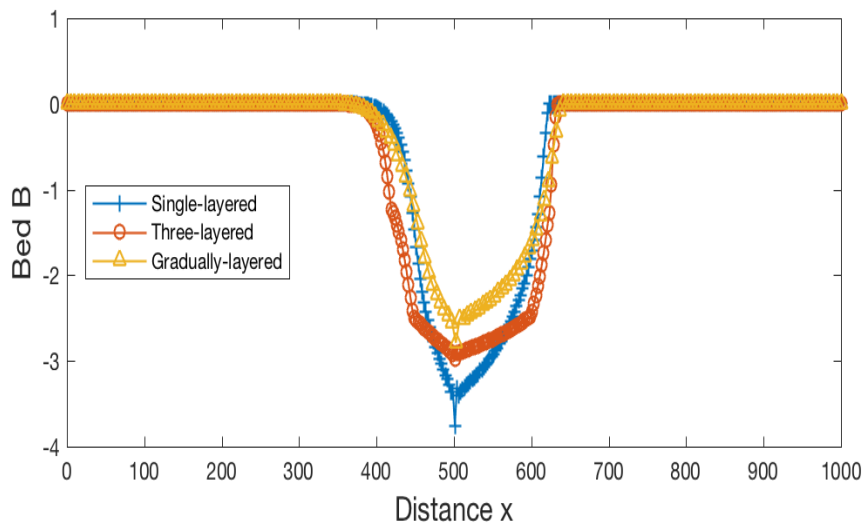


Figure 9: Comparison of bed profiles obtained for a dam-break problem over single-layered, three-layered and gradually varying bed at time $t = 20$ s.

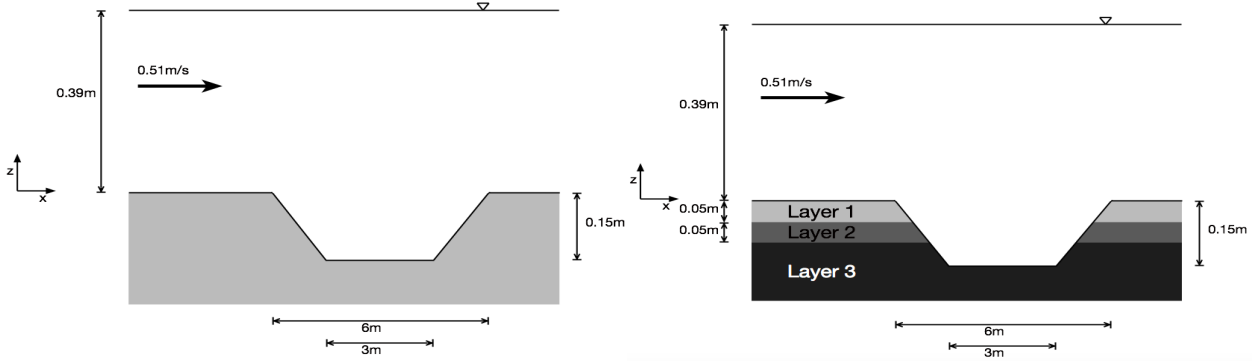


Figure 10: Schematic description of the stream flow problem over single-layered Dyke (left plot) and three-layered Dyke (right plot).

Table 3: Convergence results for the stream-flow problem over single-layered Dyke.

Δx	Minimum B	Location (x, z) of the minimum B	CPU time
0.6 m	-0.1250 m	(16.15 m, -0.1250 m)	126 min
0.5 m	-0.1173 m	(16.36 m, -0.1173 m)	254 min
0.2 m	-0.1103 m	(16.38 m, -0.1103 m)	928 min
0.15 m	-0.109 m	(16.38 m, -0.1090 m)	1736 min
0.1 m	-0.1083 m	(16.39 m, -0.1083 m)	3774 min

using the three bed configurations is presented in Figure 9. It is interesting to note that while all these cases are approximations of the same situation, very different final bed profiles are developed. This highlights the differences between assumptions made on multiple species of sediment (in the graded bed) and the discrete sediment layers, as they provide fundamentally different bed profiles. Especially with the three-layered bed where not only the magnitude but also the shape of the erosion changes. Unfortunately, there is no experimental data to validate these results against but the proposed method correctly captures the morphodynamical features.

5.2 Results for stream-flow problems

Our next concern is to examine the performance of the proposed numerical techniques for stream-flow problems over erodible beds, and also to validate the obtained numerical results against measurements for single-layered homogeneous bed. To this end we consider the test example of a stream flow over a Dyke studied in the Delft hydraulics laboratory Guan et al. (2015). Here, the experiment is carried out in a rectangular channel with a 1:10 slope as sketched in the left plot of Figure 10. The bed is assumed to be single-layered formed with Sand 4 the sediment properties of which are listed in Table 1. Initially the flow is at rest with a water height $h(0, x) = 0.39$ m and a velocity of $u(t, x) = 0.51$ m/s is set as an upstream boundary condition. For this far-field problem the erosion term is given by the formula (15).

As in the previous example we also perform a study of grid convergence for this test example of far-field sediment transport. In Table 3 we summarize the minimum value of the bed profile B , the location (x, z) where this minimum is reached, and the computational cost obtained at simulation time $t = 27000$ s. Note that for this far-field problem the mean velocity is slow compared to the

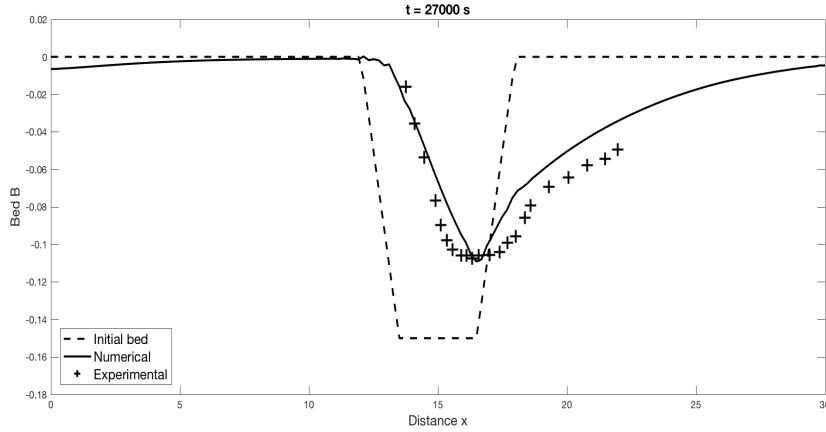


Figure 11: Comparison between numerical results and experimental data for the stream-flow problem over single-layered Dyke at time $t = 27000$ s.

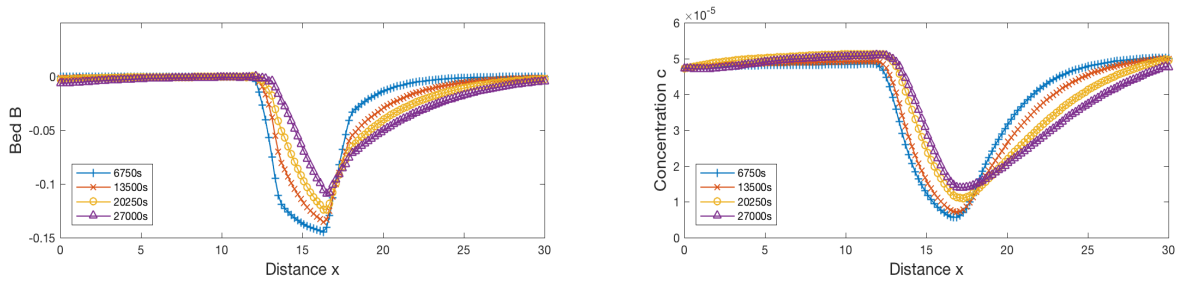


Figure 12: Time evolution of bed profile (left plot) and sediment concentration (right plot) for the stream-flow problem over single-layered Dyke.

previous test example and therefore longer simulation times are required to obtain well-developed morphodynamics. It is clear from the obtained results that using fine grids yields large CPU times for the same simulation time. Based on the results shown in Table 3 a spatial discretization with $\Delta x = 0.2$ m is considered in our study as the differences in the accuracy between this discretization and the refined ones using $\Delta x = 0.15$ m or $\Delta x = 0.1$ m are very small but the difference in the computational cost is vast.

A comparison between the computational results and experimental data has also been carried out for this test problem. In Figure 11 we compare the numerical results for the bed profile at time $t = 27000$ s to measurements reported in Guan et al. (2015). We also include in this figure the initial bed profile for comparison reasons. It is clear that the numerical and experimental results demonstrate similar morphodynamical patterns and our Riemann solver is capable to accurately capture both hydrodynamics and morphodynamics features. Both erosion and deposition effects have been numerically resolved using our approach without introducing excessive numerical diffusion or nonphysical oscillations. These effects can be clearly seen in the time evolution of bed profile and the sediment concentration shown in Figure 12. Notice that the minimum values of the bed profiles and their locations obtained using the proposed Riemann solver are similar to measurements.

It should also be pointed out that in the previous test example of far-field dam-break problems, the obtained results do not demonstrate large amounts of deposition mainly due to their high levels of scouring. Therefore, the aim of this test example of evolving flow problems is to demonstrate

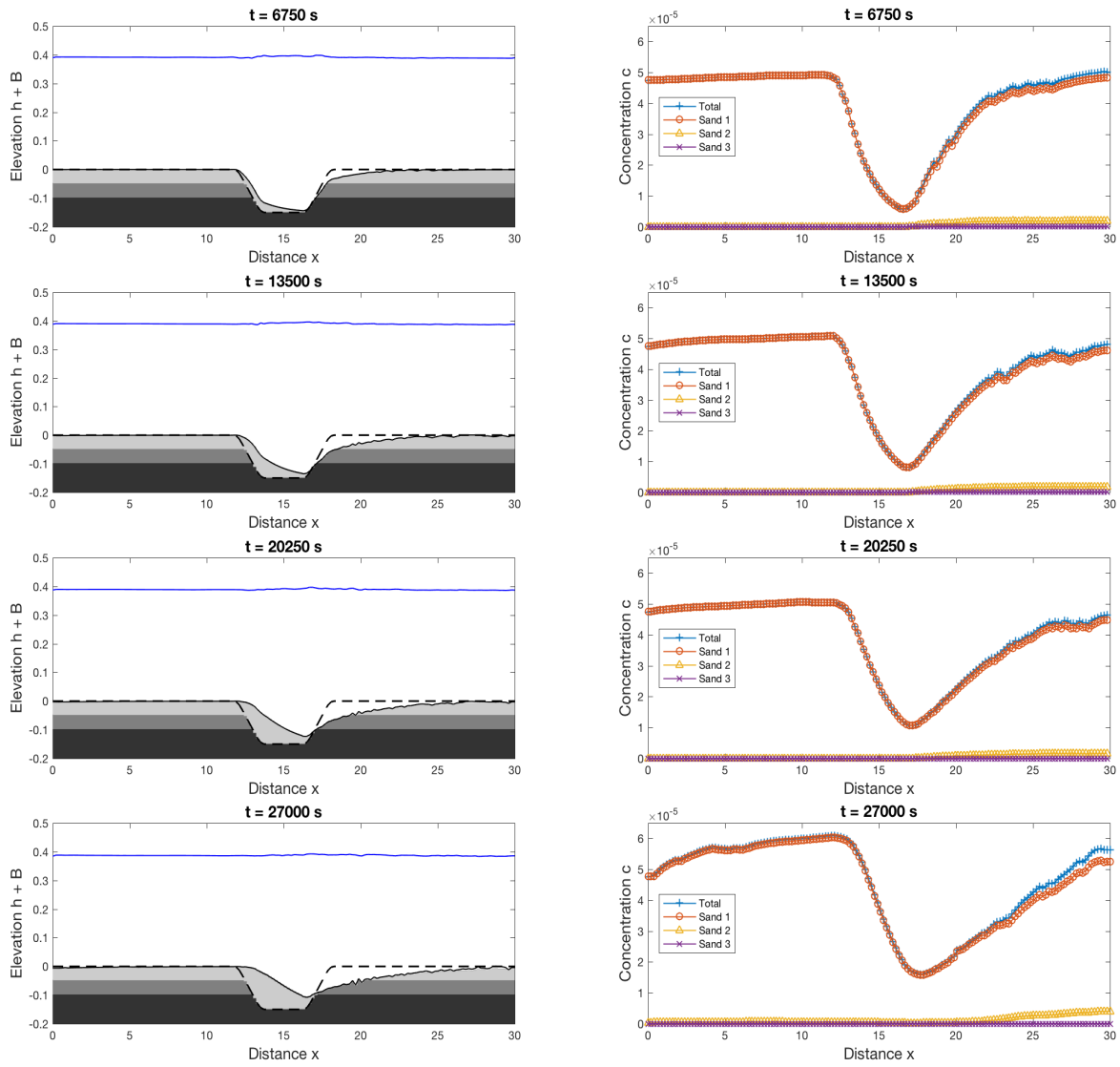


Figure 13: Bed profiles (left column) and sediment concentrations (right column) for the stream-flow problem over three-layered Dyke at four instants $t = 6750, 13500, 20250$ and 27000 s. The blue and dashed lines in the left plots refer to the water free-surface and the initial bed profile, respectively.

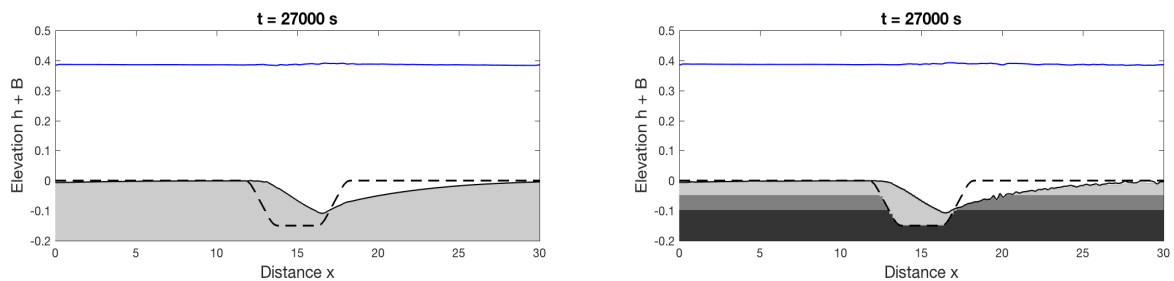


Figure 14: Bed profiles at time $t = 27000$ s obtained using single-layered bed (left) and three-layered bed (right). The blue and dashed lines in the left plots refer to the water free-surface and the initial bed profile, respectively.

the effects of deposition and specifically the phenomenon of armoring. Hence, a new test case is devised using three discrete sediment layers, where below $z = -0.050 \text{ m}$ the Sand 5 was used and below $z = -0.100 \text{ m}$ the even less erodible Sand 6 is used *i.e.*,

$$B(0, x, z) = \begin{cases} \text{Sand 4,} & \text{if } -0.05 \text{ m} \leq z < 0 \text{ m,} \\ \text{Sand 5,} & \text{if } -0.1 \text{ m} \leq z < -0.05 \text{ m,} \\ \text{Sand 6,} & \text{if } -0.2 \text{ m} \leq z < -0.1 \text{ m,} \end{cases}$$

where the associated sediment properties for Sand 4, Sand 5 and Sand 6 are given in Table 1. The computed results for the bed profiles and sediment concentrations are illustrated in Figure 13 at four different instants $t = 6750, 13500, 20250$ and 27000 s using a spatial discretization with ($\Delta x = 0.2 \text{ m}, \Delta z = 0.002 \text{ m}$). As can be observed from these results, the deposition effects on the Dyke are clearly visible as the time evolves. The variation of the bed sediments creates a very active sediment exchange between the water flow and the bed load and also produces a sharp spatial gradient of sediment concentration presented in Figure 13. As can also be seen, the water free-surface remains almost constant during the simulation times except few fluctuations over the region where the deposition occurs. It seems that, for the considered sediment conditions, erosion effects are more pronounced for the first layer of Sand 4 than for the second layer of Sand 5 and for third layer of Sand 6. For completeness we present in Figure 14 a comparison between simulations for the single-layer bed (using Sand 4 only) and the three-layered bed (using Sand 4, Sand 5 and Sand 6) at time $t = 27000 \text{ s}$. Again, for the considered sediment properties, both simulations deliver similar top bed profile but using the single-layer bed would not reveal the intermediate profiles for sedimentary beds. It is clear that by using Riemann solver, high resolution is obtained in those regions where the gradients of the bed are steep such as the moving deposition fronts.

6 Conclusions

A finite volume model has been proposed for the numerical solution of shallow water flows over multi-layered sedimentary topography. The governing equations consist of a shallow water system for the water flow and transport and suspended equations for the sediments. To model erosion and deposition we have used empirical equations for both evolving and steady-state flow situations. The vertical exchanges between the bed layers have been accounted for using a balance law for the bed elevation. The model presents a real opportunity for shallow water flows over erodible beds. The proposed model is fully coupled and it can handle an arbitrary number of layers within the bed topography. In addition, the governing equations can be formulated as a hyperbolic system of balance laws with source terms. The numerical method uses a class of predictor-corrector procedures for which the numerical fluxes are reconstructed in the predictor stage using the Jacobian matrix of the fluxes in the system followed by a corrector stage to update the solution of the system. We also consider a conservative vertical discretization of finite volume type for the multi-layered bed to allow for different soil properties forming the bed. The combined techniques offer an accurate and stable numerical solver with a well-balanced discretization of the flux gradient and the source term. The current work is the first to propose a fast and accurate finite volume model for numerical simulation of shallow water flows over multi-layered topography using vertical discretization of the sedimentary bed.

The numerical performance of the proposed solver is examined for several test examples, including a dam-break problem over multi-layered erodible beds and a stream-flow problem over multi-layered erodible Dyke. We have also compared the numerical results obtained using our approach for single-layered beds to experimental measurements in both evolving and steady-state

flow simulations. In all presented results, the proposed solver has exhibited accurate predictions of both, the water free-surface and the bed topography with correct conservation properties and stable representations of free-surface response to the multi-layered erodible beds. The presented results make it promising to be applicable also to real situations where, beyond the many sources of complexity, there is a more severe demand for accuracy in predicting the morphodynamics, which must be performed for a long time. Future work will concentrate on developing high-order discretization methods and the extension of these techniques to shallow water flows over sedimentary topography in two space dimensions.

References

- Abbott, M. (1979), *Computational hydraulics: Elements of the theory of free surface flows*, Fearon-Pitman Publishers.
- Abderrezzak, K., Moran, A., Mosselman, E., Bouchard, J., Habersack, H. and Aelbrecht, D. (2013), ‘A physical, movable-bed model for non-uniform sediment transport, fluvial erosion and bank failure in rivers’, *Journal of Hydro-environment Research* **8**, 95–114.
- Alcrudo, F. and Benkhaldoun, F. (2001), ‘Exact solutions to the Riemann problem of the shallow water equations with a bottom step’, *Computers & Fluids*. **30**, 643–671.
- Benkhaldoun, F., Sari, S. and Seaid, M. (2012), ‘A flux-limiter method for dam-break flows over erodible sediment beds.’, *Applied Mathematical Modelling* **36**, 4847–4861.
- Brownlie, W. (1981), ‘Prediction of flow depth and sediment discharge in open channels’, *Report Number KH-R-43A. Keck Laboratory of Hydraulics and Water Resources, California Institute of Technology*.
- Cao, Z. and Carling, P. (2002), ‘Mathematical modelling of alluvial rivers: reality and myth. part I: General overview.’, *Water Maritime Engineering* **154**, 207–220.
- Cao, Z. and Pender, G. (2004), ‘Numerical modelling of alluvial rivers subject to interactive sediment mining and feeding.’, *Advances in Water Resources* **27**, 533–546.
- Cao, Z., Pender, G. and Carling, P. (2006), ‘Shallow water hydrodynamic models for hyperconcentrated sediment-laden floods over erodible bed.’, *Advances in Water Resources* **29**, 546–557.
- Cao, Z., Pender, G., Wallis, S. and Carling, P. (2004), ‘Computational dam-break hydraulics over erodible sediment bed.’, *Journal of Hydraulic Engineering* **67**, 149–152.
- Capart, H. and Young, D. (1998), ‘Formation of jump by the dam-break wave over a granular bed’, *Journal of Fluid Mechanics* **372**, 165–187.
- Chen, S., Yang, C. and Tsou, C. (2017), ‘Bedform development and its effect on bed stabilization and sediment transport based on a flume experiment with non-uniform sediment’, *International Journal of Sediment Research* **32**, 305–312.
- Grass, A. (1981), ‘Sediment transport by waves and currents.’, *SERC London Cent. Mar. Technol.* **29**.
- Guan, M., Wright, N. and Sleigh, P. (2015), ‘Multimode morphodynamic model for sediment-laden flows and geomorphic impacts’, *Journal of Hydraulic Engineering* **141**, 04015006.
- Hu, P. and Cao, Z. (2009), ‘Fully coupled mathematical modeling of turbidity currents over erodible bed’, *Advances in Water Resources* **32**, 1–15.

- Kondolf, G., Gao, Y., Annadale, G., Morris, G., Jiang, E., Zhang, J., Cao, Y., Carling, P., Fu, K., Gui, Q., Hotchkiss, R., Peteuil, C., Sumi, T., Wang, H., Wang, Z., Wei, Z., Wu, B., Wu, C. and Yang, C. (2014), ‘Sustainable sediment management in reservoirs and regulated rivers: Experiences from five continents’, *Earth’s Future* **2**, 256 – 280.
- Kozyrakakis, G. (2016), ‘Numerical modeling of sediment transport applied to coastal morphodynamics’, *Applied Numerical Mathematics* **104**, 30–46.
- Li, S. and Duffy, J. (2011), ‘Fully coupled approach to modeling shallow water flow, sediment transport and bed evolution in rivers.’, *Water Resources Research* **47**, 1–20.
- Liang, D., Lin, B. and Falconer, R. (2003), ‘A boundary-fitted numerical model of flood routing with shock-capturing capability’, *Journal of Hydraulics* **332**, 447–486.
- Liu, X. and A., B. (2017), ‘A coupled numerical model for water flow, sediment transport and bed erosion’, *Computers and Fluids* **154**, 273–284.
- Meyer-Peter, E. and Müller, R. (1948), ‘Formulas for bed-load transport.’, *Report on 2nd meeting on international association on hydraulic structures research* **1**, 39–64.
- Mohtar, W., Junaidi, J., Sharil, S. and Mukhlisin, M. (2016), ‘Representative sediment sizes in predicting the bed-material load for nonuniform sediments’, *International Journal of Sediment Research* **31**, 79–86.
- Paphitis, D. (2001), ‘Sediment movement under unidirectional flows: an assessment of empirical threshold curves.’, *Coastal Eng* **43**, 227–245.
- Rowan, T. and Seaid, M. (2016), ‘Development and verification of a finite volume model for hydraulics over multi-layered erodible beds’, *Proceedings of the 8th International Conference on Scour and Erosion* **1**, 119–130.
- Rubey, W. (1933), ‘Settling velocity of gravel, sand, and silt particles’, *American Journal of Science* **148**, 325–338.
- Sahmim, S., Benkhaldoun, F. and Alcrudo, F. (2007), ‘A sign matrix based scheme for quasi-hyperbolic non-homogeneous pdes with an analysis of the convergence stagnation problem’, *Journal of Computational Physics* **226**, 1753–1783.
- Sanford, L. (2008), ‘Modelling a dynamically varying mixed sediment bed with erosion, deposition, bioturbation, consolidation, and armouring.’, *Computers & Geosciences* **34**, 1263–1283.
- Shields, A. (1936), Anwendung der Ähnlichkeitsmechanik und der Turbulenzforschung auf die Geschiebebewegung., PhD thesis, Mitteilung der preussischen Versuchsanstalt für Wasserbau und Schiffbau.
- Simpson, G. and S., C. (2006), ‘Coupled model of surface water flow, sediment transport and morphological evolution’, *SIAM J. Numer. Anal.* **21**, 1600–1614.
- Siviglia, A., Stecca, G. and Blom, A. (2017), *Modeling of mixed-sediment morphodynamics in gravel bed rivers using the active layer approach: Insights from mathematical and numerical analysis. In Gravel-bed Rivers: Processes and Disasters*, Wiley.
- Terzaghi, K., Peck, R. and Mersi, G. (1996), *Soil Mechanics in Engineering Practice*, John Wiley & Sons Publishers.
- Toro, E. (1999), *Riemann Solvers and Numerical Methods for Fluid Dynamics*, Springer Verlag.

- Van Rijn, L. (1984), 'Sediment pick up functions.', *Journal of Hydraulic Engineering* **110**, 1494–1502.
- Van Rijn, L. (2007), 'Unified view of sediment transport by currents and waves. I : Initiation of motion, bed roughness, and bed-load transport', *Journal of Hydraulic Engineering* **113**, 649–667.
- Vercruyssen, K., Grabowski, R. and R., R. (2017), 'Suspended sediment transport dynamics in rivers: Multi-scale drivers of temporal variation', *Earth-Science Reviews* **166**, 38–52.
- Wu, W. and Wang, S. (2006), 'Formulas for sediment porosity and settling velocity', *Journal of Hydraulic Engineering* **132**, 858–862.
- Zhang, Q., Zhou, X., Wang, J. and Guo, J. (2017), 'Wave-induced seabed response around an offshore pile foundation platform', *Ocean Engineering* **130**, 567–582.